Lateral Diffusion and Retrograde Movements of Individual Cell Surface Components on Single Motile Cells Observed with Nanovid Microscopy

Mark de Brabander,* Ronny Nuydens,‡ A. Ishihara,§ Bruce Holifield,§ Ken Jacobson,§ Hugo Geerts‡

Departments of *Cellular Biology and Pathology and ‡Physiology, Life Sciences, Janssen Research Foundation, Beerse, Belgium; and §Department of Cell Biology and Anatomy, School of Medicine, University of North Carolina at Chapel Hill, Chapel Hill, North Carolina 27599

Abstract. A recently introduced extension of video-enhanced light microscopy, called Nanovid microscopy, documents the dynamic reorganization of individual cell surface components on living cells. 40-μm colloidal gold probes coupled to different types of poly-L-lysine label negative cell surface components of PTK_2 cells. Evidence is provided that they bind to negative sialic acid residues of glycoproteins, probably through nonspecific electrostatic interactions. The gold probes, coupled to short poly-L-lysine molecules (4 kD) displayed Brownian motion, with a diffusion coefficient in the range 0.1–0.2 $\mu m^2/s$. A diffusion coefficient in the 0.1 $\mu m^2/s$ range was also observed with 40-nm gold probes coupled to an antibody against the lipid-linked Thy-1 antigen on 3T3 fibroblasts. Diffusion of these probes is largely confined to apparent microdomains of 1–2 μm in size. On the other hand, the gold probes, coupled to long poly-L-lysine molecules (240 kD) molecules and bound to the leading lamella, were driven rearward, toward the boundary between lamelloplasm and perinuclear cytoplasm at a velocity of 0.5–1 μm/min by a directed ATP-dependent mechanism. This uniform motion was inhibited by cytochalasin, suggesting actin microfilament involvement. A similar behavior on MO cells was observed when the antibody-labeled gold served as a marker for the PGP-1 (GP-80) antigen. These results show that Nanovid microscopy, offering the possibility to observe the motion of individual specific cell surface components, provides a new and powerful tool to study the dynamic reorganization of the cell membrane during locomotion and in other biological contexts as well.

In highly mobile cells, an impressive reorganization of cell surface material occurs, especially at the leading edge (Abercrombie et al., 1970; Bretscher, 1984). This movement is correlated to the activity of the leading lamella, the protrusion of the lamellipodia, and the retraction of the trailing edge in the global movement of the cell. Another important issue in cell surface organization is lateral phase separation and the existence of putative microdomains (Yechiel and Edidin, 1987). The dynamic onset of lateral phase separation, for instance, is a prime parameter in ischemia-induced pH shifts (Verkleij and Post, 1987). Different models have been proposed for the dynamic redistribution of cell membrane proteins (Bretscher, 1983; Goldstein and Wiegel, 1988; Ishihara et al., 1988). An accurate assessment of membrane protein organization is of prime importance in distinguishing these models. Clearly there is a need for an accurate dynamic visualization of specific components on the cell surface.

Thus far, the dynamic reorganization of cell surface components on living cells in the light microscope could only be investigated using averaging techniques such as digitized fluorescence microscopy or fluorescence recovery after photobleaching (FRAP).[1] These techniques average the motion of a number of components, sometimes driven by an imposed concentration gradient. In that way, the subtle and heterogeneous spatial differences of motion are often not revealed. In addition, the noise usually restricts the amount of information. In the FRAP method, for instance, the interpretation of the experiment is hampered by the very small difference between Brownian motion and uniform flow, which usually is buried in the noise. Progress towards answers on questions concerning mechanism and significance of cell surface reorganization would be facilitated if motion of individual and specific membrane components could be tracked.

The motion of individual large spheres (1 μm and larger) on fibroblast cells was followed with cinemicroscopy, and studied in great detail (Abercrombie et al., 1970; Harris and

1. *Abbreviations used in this paper*: Au40, 40-nm colloidal gold particles; DMJ, 1-deoxymannojirimycin; FRAP, fluorescence recovery after photobleaching; G40, Gold 40; PEG, polyethyleneglycol; p-L-l, poly-L-lysine; PVP, polyvinylpyrrolidine; TX-100, Triton X-100.

Dunn, 1972; Dembo and Harris, 1981). In recent years, technological advances in low-light level microscopy allowed the motion of individual fluorescently labeled low density lipoprotein complexes on macrophages to be followed (Gross and Webb, 1986). However, fluorescence imaging is hampered by the bleaching of the probe and concomittant phototoxicity. These factors usually restrict time resolution. Recently, video microscopy was used to study the dynamic reorganization of Con A–40-nm colloidal gold (Au) on living cells (Sheetz et al., 1989; Kucik et al., 1989). In this report, we show that Nanovid microscopy, which is the application of video-enhanced light microscopy to specific colloidal gold probes (de Brabander et al., 1986, 1988; Geerts et al., 1987), can detect the mobility of individual markers on the cell surface in real time on living cells. We used 40-nm colloidal gold particles, coupled to poly-L-lysine (p-L-l) molecules of 4- and 240-kD, respectively, to detect negatively charged cell surface residues. In addition, we visualized the redistribution of the major membrane glycoprotein PGP-1 antigen (Hughes et al., 1981) on MO cells, by use of a monoclonal antibody coupled to 40-nm gold particles. Furthermore, the Brownian motion of the Thy-1 membrane glycoprotein on 3T3 fibroblast was studied in detail with a 40-nm colloidal gold probe, coupled to a monoclonal antibody against Thy-1. It is shown that these gold probes, coupled to different classes of cell surface components, can reveal lipid-mediated fast Brownian motion dynamics as well as an active, microfilament-mediated reorganization of the cell membrane components.

Materials and Methods

Cell Cultures

PtK_2, MO, and 3T3 fibroblast cells were routinely cultured in MEM supplemented with nonessential amino acids and 10% FCS in a 5% CO_2 atmosphere. Before use, at least 48 h after plating, the cells were washed with and transferred to PBS containing 1 g/liter glucose, with or without drug. This was done at least 15 min before addition of the gold probes.

Gold Particles for Nanovid Microscopy

40-nm gold particles were prepared and stabilized with polyethyleneglycol (PEG) and BSA as described before (De Mey, 1983). These particles have a negative surface charge. Positively charged gold particles were prepared by incubating this PEG/BSA-stabilized 40-nm Au sols (OD of 38.4 at λ_{max} of 530 nm) with p-L-l hydrobromide of 4 or 240 kD for 60 min at room temperature. The final concentration of p-L-l was 100 μg/ml, unless otherwise indicated.

Direct coupling of monoclonal antibodies to the colloidal gold probes was performed using polyvinylpyrrolidine K15 (PVP, 10 kD; Aldrich Chemical Co., Milwaukee WI) and 0.1% gelatin as stabilizers. The probes were added to the preparation with 50 μl of a 1:20 dilution in PBS with 1 g/liter glucose. As a rule, excess gold particles were removed after 15 min by perfusion with PBS + 1 g/liter glucose. All compounds used were dissolved in DMSO (5 mg/ml) and diluted in PBS containing 1 g/liter glucose for the short-term incubations.

For the long-term experiments drugs were diluted in tissue culture medium. At the final concentrations used, the solvent had no apparent effects.

Video Microscopy

Preparations were made by inverting the coverslip with the cells on a microscope slide using Parafilm strips as spacers. The microchamber was sealed with Valap (vaseline, lanoline, paraffin, 1/3 of each).

The Reichert Polyvar microscope was equipped with a universal condenser (NA = 1.30) and a 100× planapoobjective (NA = 1.32). Köhler illumination was achieved throughout the observation period using oil immersion on both the condenser and objective lens. Temperature of the stage was kept at 37 ± 1°C by an airstream incubator. Observations were made with transmitted light of differential interference contrast using the full numerical aperture of the system, by using the green line (wavelength = 546 nm) of a 100-W halogen lamp or a 200-W mercury arc. The image was projected on the camera of a video microscope system (model C1966; Hamamatsu Phototonics K.K., Hamamatsu City, Japan). The videosignal was fed into a U-matic videorecorder (model VO5850P; Sony). Recordings were made in real-time or in time-lapse mode by using an animation control unit (model HC580; EOS Electronics AV, Barry, UK). As a rule, the recorder was instructed to grab two frames every 10 s. To assess the effect of membrane alterations on colloidal gold density, well-defined regions of cells were observed on the microscope. Manual counts of colloidal gold particles were compared before and after treatment. Living cells incubated for 15–30 min with p-L-l Au were treated with 0.05% Triton X-100 (TX-100) in PBS or with 0.15% TX-100 in buffer S (60 mM Pipes, 25 mM Hepes, 10 mM EGTA, 1 mM $MgCl_2$, pH 6.9). In all cases, TX-100 treatment was performed under the microscope.

Immunofluorescence and EM

For immunofluorescence, cells were fixed with 1% glutaraldehyde in Pipes buffer (HBSS, 5 mM Pipes, 2 mM $MgCl_2$, 2 mM EGTA, pH 6.0) for 10 min and permeabilized with 0.5% TX-100 for 30 min. The cells were sequentially stained with antiactin antibody (Langanger et al., 1984) and monoclonal antitubulin (Kilmartin, 1982), and then a mixture of TRITC-coupled goat anti-rat immunoglobulins and FITC-coupled goat anti-rabbit immunoglobulins. Coverslips were mounted in Gelvatol with 100 mg/ml DABCO (1,4-diazabicyclo[2.2.2]octane) to reduce fading.

For EM, cells were seeded on MS-122-coated coverslips. Preparations were treated with 2% osmium tetroxide for 1 h at 4°C, after which they were impregnated for 1 h with 0.5% uranyl acetate. After dehydration in a graded series of ethanol, they were embedded in Epon. Selected cells on ultrathin sections were viewed in an electron microscope (model EM401; Philips Electronic Instruments Inc., Mahway, NJ).

Charge Measurements

Charge measurements of the gold complexes were performed on an electrophoretic laser light scattering instrument (model 3000, Pen Kem, Inc., Bedford Hills, NY) to determine electrophoretic mobility, which is proportional to the Z potential. Assuming that the Z potential is not very different from the surface potential Ψ, the relation between surface charge density (σ) and Z is (Grahame, 1947)

$$\sigma = 0.35 \sinh (0.02\ Z)\ \mu C/cm^2. \quad (1)$$

Quantitative Measurements of Colloidal Gold Motion

For the quantitative analysis of motion, the videotape is read into the external video input of the Hamamatsu processor, digitized by an 8-bit A/D convertor and transferred via a direct memory access interface to a MicroVax II. The video recorder is interfaced to the Vax computer by means of a video device driver (OTOMATE, Netherlands). This allows the operator to automatically take in frames with a constant interframe time, which, depending on the experiment, ranges from 300 μs to 1 s. Because of the particular character of the gold probe, the particles on the cell surface can be located exactly by a gray-scale morphology algorithm in the video image (Sternberg, 1986; de Brabander et al., 1989).

When the labeling density was not too high, the movements of the gold probes were studied with the Nanovid tracking technique (Geerts et al., 1987*b*). Motion was quantified using the relationship between x^2 and the elapsed time (T); i.e.,

$$x^2 = 4DT + v^2T^2, \quad (2)$$

where x is the displacement, D the diffusion coefficient, and v the linear velocity. Typically between 10 and 20 frames were used to calculate the regression line. χ^2 statistics were used to differentiate between the linear case of pure Brownian motion or the parabolic relationship for a mixed motion.

Tracing (which reveals the long-term displacement of individual components, by accumulating subsequent images in real-time and subtracting a static background) was performed with the TRACE mode of an image processor system (model C1966; Phototonic Microscopy Inc., Oak Brook,

Table I. Mean Surface Charge Measurements of Different p-I-L Au40 Probes As Measured by Electrophoretic Light Scattering

Probe	p-I-l density	Concentration p-I-l	Mobility	Z potential	Surface
e⁻/1,000 nm²		*g/liter*		*μm/s·kV*	*mV*
G40		–	−33.0	−44	−20
G40-P/B	–		−21.0	−27	−13
G40-P/B	4-kD	0.1	−4.8	−6	−2.4
G40-P/B	4-kD	1.0	−5.2	−6	−2.4
G40-P/B	240-kD	0.1	−8	−9	−3.6
G40-P/B	240-kD	1.0	+9	+11	+4.4

Data are given for PEG/BSA (P/B) stabilizers and different incubation concentrations of p-L-l. All incubations were performed in identical conditions as for the video microscopy experiments. The surface density is calculated according to Eq. 1. Addition of longer p-I-l molecules reverts the original negative charge on the stabilized Au sol, as evidenced by the less negative Z potential. In addition, increasing concentrations of p-I-l results in more explicit charge reversions.

IL). The histogram distribution out of such a TRACE image (the area covered by one particle in its diffusion behavior over a certain period is proportional to the square of its displacement) as compared to the calculated probability functions for free two-dimensional diffusion (Crank, 1974) is as follows:

$$P(x,t) = \exp(-x^2/4Dt/(4\pi Dt)^{1/2} \quad (3)$$

In situations where the density of gold label was too high for individual particle tracking, movements were analyzed over 500 to 1,000 image frames by Nanovid Correlation Spectroscopy (Geerts et al., 1987*a*). Briefly, some 20 to 30 "windows" of size ω are outlined on the surface of the cell in the video experiment, and the concentration of gold probes in each window is measured for each frame. The "instantaneous" concentration of gold particles fluctuates, due to random diffusion in and out of each window. The average decay time for each fluctuation, T_R, is calculated to be $\omega^2/4D$. We therefore get a spectrum of diffusion constants (D) in different points over the cell.

Results

Characterization of the Binding of Various Gold Probes to the Cell Surface

The intrinsic negative charge on colloidal gold particles is neutralized and reversed by the binding of p-L-l to their surface. The mean charge density, as measured by electrophoretic light scattering is a weighted average over a large distribution of charges. Table I shows that the average charge on PEG/BSA-stablized gold probes is negative. However, this charge can be decreased and even reversed by incubation with different sized p-L-l in various concentrations. It is clear from this table that the 4- and 240-kD p-L-l–coated gold probes have similar charge densities.

In addition, control experiments showed no labeling of the cell surface even after prolonged incubations with concentrated negatively charged PEG/BSA Au sol. Sometimes a particle was seen touching the cell membrane. It moved on the membrane in a Brownian fashion for a short period (5–10 s) and detached again. Apparently, only the fraction of the gold probes carrying positive charges was selected out to bind to the negative sialic acid residues.

Further information on the binding sites of the p-L-l Au conjugates was deduced by the effect of various plasma membrane alterations. First, plasma membrane was removed by incubation with TX-100. 4-kD p-L-l Au was partly removed (60%) by treating the cells with TX-100–containing buffers. Accumulations on cell contacts did not completely disappear but the label density was strongly reduced. The 240-kD p-L-l Au particles showed a higher resistance to the TX-100 treatment as only 18% of the label was removed. In particular, accumulations formed on transition zones and cell–cell contacts stayed at their location, often near actin filaments. When these lysis conditions were applied to cells labeled with the fluorescent lipid probe Dil-C_{18}-3, all membrane-associated fluorescence was removed.

Neither 4- or 240-kD p-L-l Au on cells fixed by 1% glutaraldehyde after addition of the positively charged particles could be removed by TX-100 treatment (up to 2%). When cells were first fixed, labeled with positively charged particles, and then treated with TX-100, 80% of the 4-kD p-L-l Au was removed while the 240-kD p-L-l Au particles remained on the cell surface.

Incubation of the cells with 20 μg/ml trypsin in CaMg-free PBS removed the 4-kD p-L-l Au but had no effect on the 240-kD p-L-l Au.

Digestion with neuraminidase from *Vibrio cholerae* (Skutelsky and Roth, 1987), to remove negatively charged sialic acid residues, or a 48-h treatment with 1-deoxymannojirimycin (DMJ), a mannosidase inhibitor (Fuhrmann et al., 1985), had no effect on the label efficiency or behavior of the 240-kD p-L-l Au (Table II). Both compounds, however, strongly reduced the label density of the 4-kD p-L-l Au (Table II and Fig. 1 *d*).

Finally, binding was unaffected by precooling to 8°C (Table II). Gold probes labeled with monoclonal antibodies to PGP-1 or Thy-1 are assumed to directly interact with their respective cell surface antigens. Cells not expressing these antigens (PtK_2 for PGP-1 or MO for Thy-1) indeed showed little or no gold particle binding.

4-kD p-L-l Au40 Binds to Surface Components That Undergo Random Lateral Diffusion

When 4-kD p-L-l Au40 (40-nm gold particles) was added to living PtK_2 cells, an evenly distributed label on the cell surface was obtained (Fig. 1 *a*). The affinity of the gold probes for the cells was much higher than for the glass sur-

Table II. Density of p-L-l Au40 Labeling in Different Conditions (n particles/100 μm²)

Condition	Probe	Density/100 μm²
Control (100 μg/ml)	4-kD	97
Control (10 μg/ml)	4-kD	23
Control (100 μg/ml)	240-kD	82
Control (10 μg/ml)	240-kD	14
Neuraminidase	240-kD	64
Neuraminidase	4-kD	13
Schliwa	240-kD	80
Schliwa	4-kD	66
DMJ	240-kD	68
DMJ	4-kD	38
8°C	4-kD	105

Control labeling is given for two different p-L-l incubation concentrations. Neuraminidase, DMJ, and Schliwa treatment are described in the text. The density (d) is calculated from the mean distance (r) between nearest neighbors, with the formula $d = 100/r^2$.

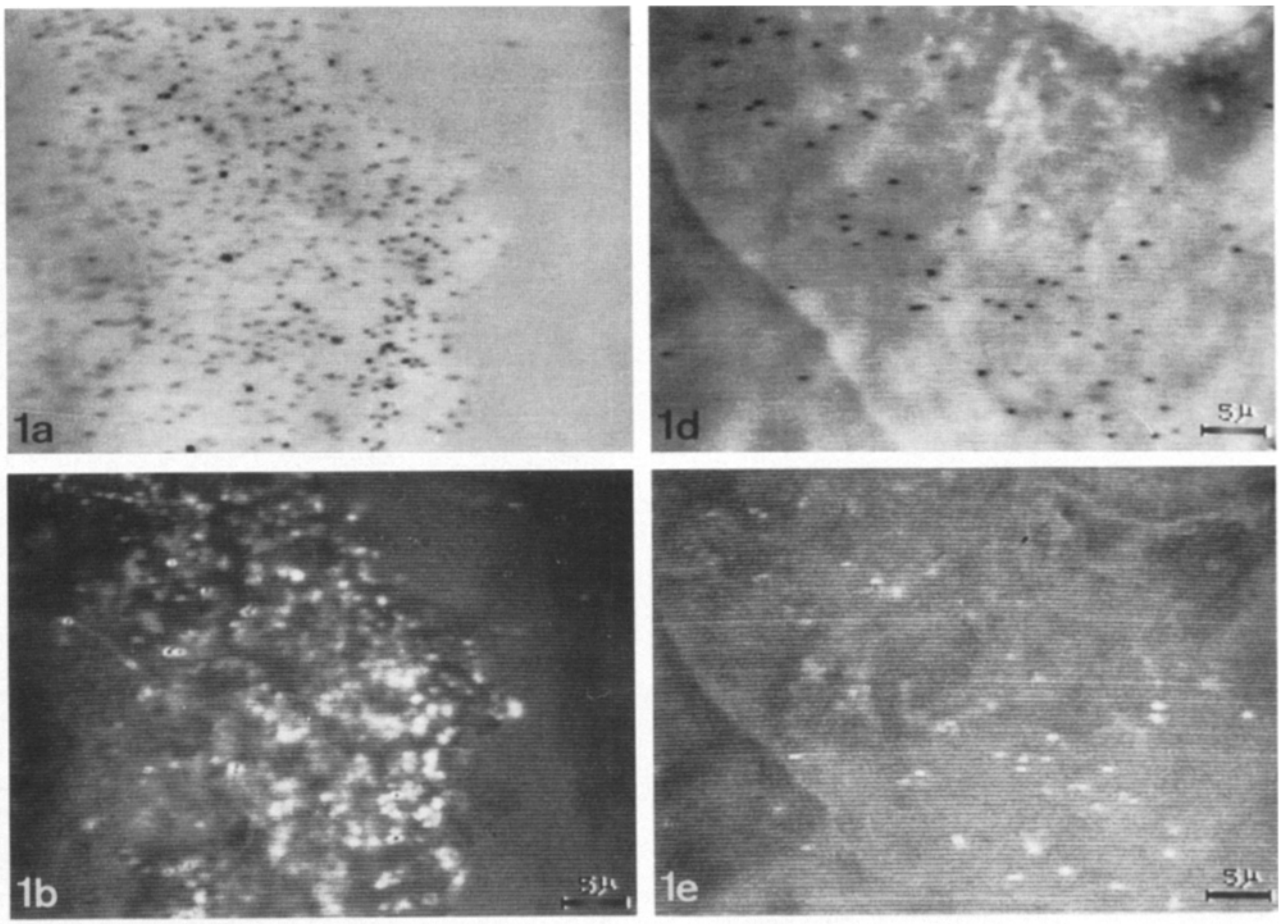

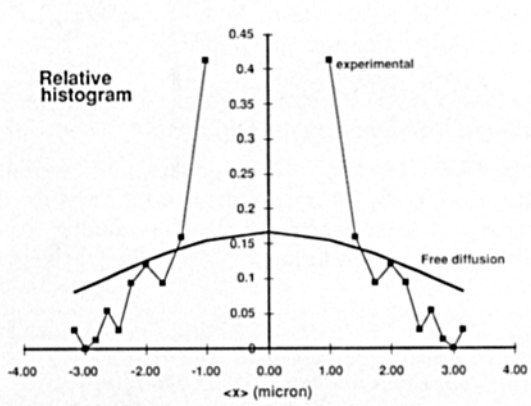

1c

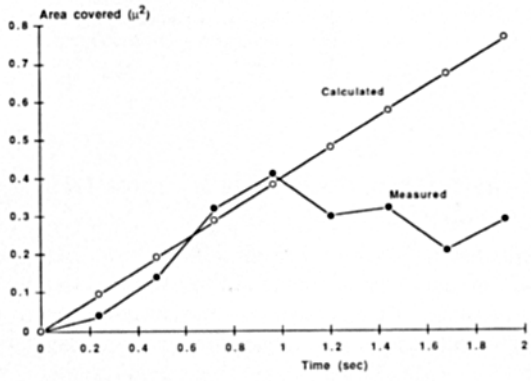

1f

Figure 1. The behavior of 4-kD p-L-l Au40 on PtK_2 cells suggest restricted diffusion in two experimental conditions with different probe densities. (*a*) Bright-field image of a PtK_2 cell with normal density of colloidal gold (97 particles/100 μm^2). (*b*) TRACE image of a 30-s sequence from the same experiment. The white blobs are the areas covered by the moving particles within this 30 s. (*c*) Histogram of the areas covered in 30 s calculated from the TRACE image. Comparison with the calculated distribution, assuming a calculated free diffusion coefficient of 0.3 $\mu m^2/s$ (Eq. 3), shows that, according to "free" diffusion, the particles should have covered a much larger area. Hence, their diffusion seems hindered or "corraled." (*d*) Bright-field image of a PtK_2 cell with a much lower density of colloidal gold (38 particles/100 μm^2) on a DMJ-treated PtK_2 cell. (*e*) TRACE image of a 30-s sequence from this experiment. Observe the areas covered by the particles in this time period. (*f*) x^2 vs. T relation of a single 4-kD gold probe in this DMJ experiment. At this lower probe density, the effect of restricted diffusion is evident as the deflection in the curve at longer times.

Table III. Results of Brownian Motion Analysis of Collodial Gold in Different Conditions and with Different Probes

Experiment	Prove	n	D ($\mu m^2/s$)
Control	4-kD	14	0.31 ± 0.11
Sodium azide	4-kD	14	0.36 ± 0.09
Sodium azide	240-kD	13	0.12 ± 0.04
Chlorpromazine (100 μM)	240-kD	13	0.14 ± 0.11
Cytochalasin B	4-kD	11	0.29 ± 0.14
8°C (T)	4-kD	68	0.04 ± 0.06
37°C (T)	Thy-1	89	0.19 ± 0.15

The mobilities are calculated by means of the Nanovid correlation spectroscopy analysis (see text). Diffusion coefficient is averaged over a number of windows (n) on the cell surface. In the condition of 8°C and of the Thy-1 probe, we were able to analyze the motion behavior with Nanovid tracking because of the low density of collodial gold. In this last case, the number of analyzed movements is indicated.

face. Most of the membrane-bound particles underwent apparent Brownian motion on the cell surface which was markedly diminished by reduced temperature but unaffected by ATP depletion or disruption of the actin cytoskeleton by cytochalasin B (Table III). Particles treated with 10 μg/ml 4-kD p-L-l all showed Brownian motion but the label density was low when compared with 100 μg/ml (Table II). When incubated with 1 mg/ml 4-kD p-L-l a mixture of moving and fixed particles was seen on the cell surface. No aggregates or accumulations were formed on the cell surface. After 30 min cell–cell contacts were accentuated by particles assuming fixed positions in these regions. These "accumulations" were presumably formed by particles diffusing to the contact where they were trapped. Occasionally particles were seen to leave these accumulations and to resume diffusive motion. The large majority of the gold particles remained on the surface for up to 4 h. Very infrequently gold particles were endocytosed in vesicles that subsequently migrate through the cytoplasm in a saltatory fashion (data not shown).

When 4-kD p-L-l Au40 was applied to prefixed cells, only ~6% of the bound particles exhibited Brownian motion and the gold did not accumulate in contact areas.

The diffusion coefficients as calculated from the Nanovid correlation spectroscopy analysis covered a 2–3-fold range. In addition, in cases where the density was much lower (for instance by using colloidal gold probes labeled with 10 μg/ml p-L-l), a diffusion coefficient could be calculated from the slope in the x vs. T relation (Fig. 1 f). On the TRACE images (Fig. 1, b and e), the white clusters are areas (proportional to the x^2) covered in 30 s by individual gold particles. The probability distribution, calculated from these TRACE images, are compared with the probability distribution expected for free diffusion (Fig. 1, c and e). It is clear that the gold particles were unable to walk over large distances, as predicted by the free diffusion model. This feature of hin-

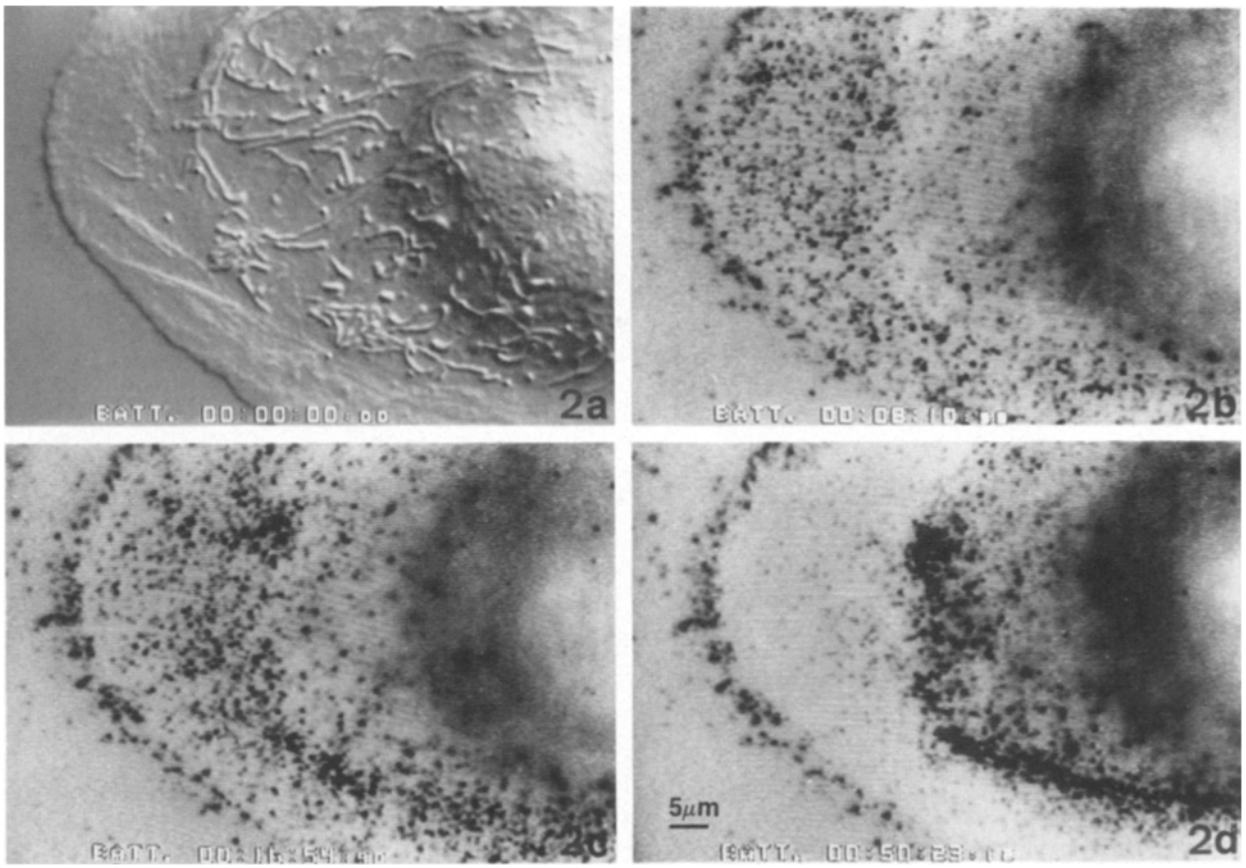

Figure 2. The behavior of 240-kD p-I-L Au40 on PtK_2 cells. (a) Nomarski interference contrast picture of a cell, before addition of colloidal gold probes. Notice the clear transition between flat lamelloplasm and organelle-rich cytoplasm. (b) Bright-field image, a few minutes (8 min 10 s) after labeling, shows a uniform label, which is more pronounced on the lamelloplasm. (c and d) Bright-field images, taken at later times, indicate the steady uniform motion of the gold label toward the transition zone between lamelloplasm and cytoplasm.

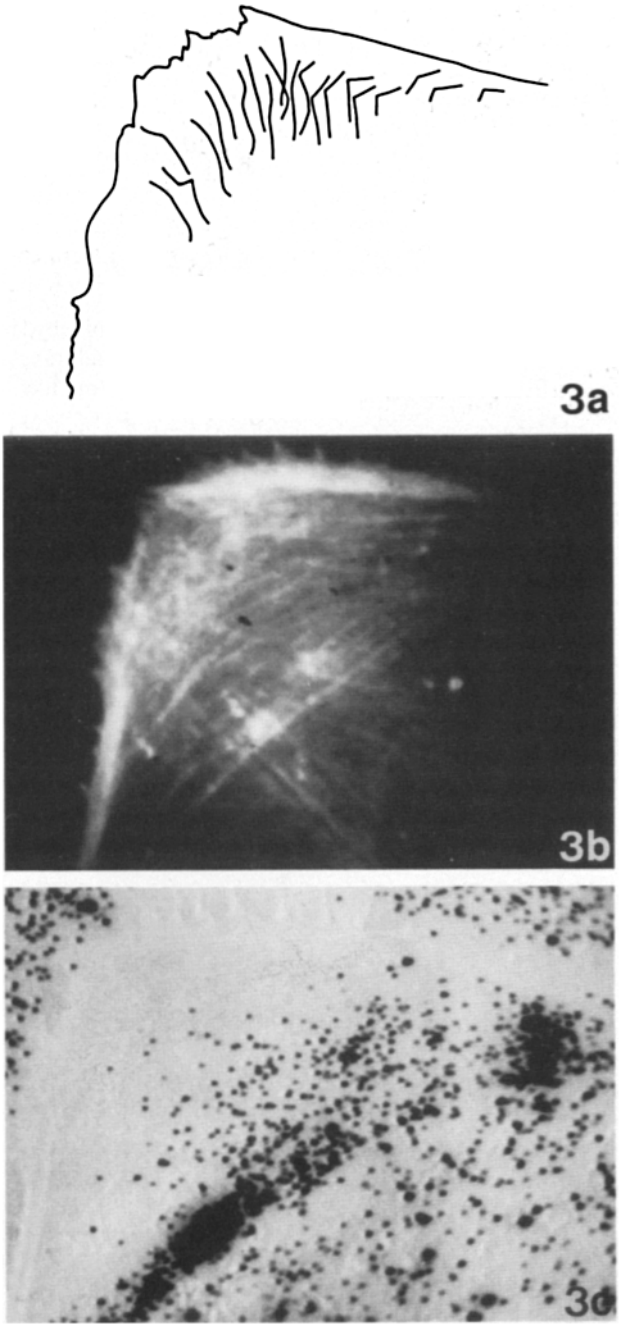

Figure 3. The movement of 240-kD p-L-l Au40 is associated with actin filaments. (*a*) Tracings of the motion of different colloidal gold particles, the directed motion is from the periphery towards the cell nucleus. (*b*) Staining of the same cell with antiactin antibody after 1 h of accumulation. Arcs of microfilaments are parallel to the cell periphery. (*c*) Bright-field image of 240-kD p-L-I complexes in the same cell just before fixation.

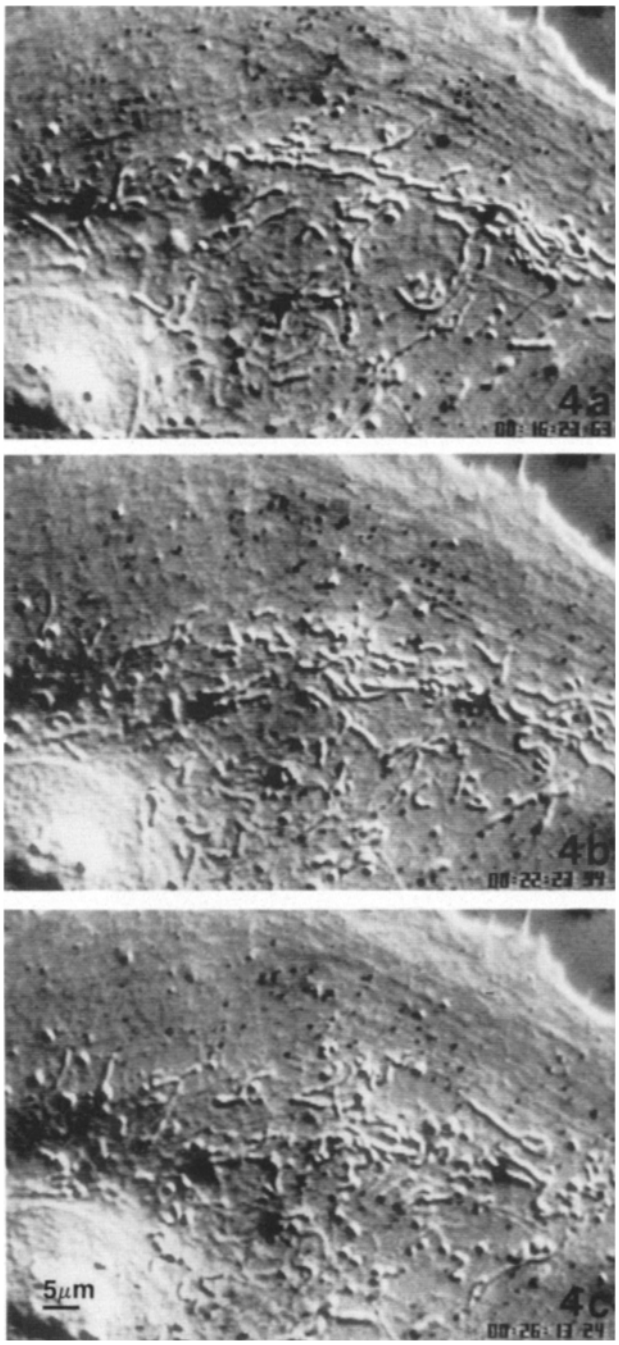

Figure 4. The association of 240-kD p-L-l Au40 with arcs of microfilaments in cells. (*a–c*) Nomarski interference contrast images at different times of cells labeled with gold. The gold is visible as small black dots, associated with bundles of parallel cytoskeletal components, probably microfilaments. In time-lapse video, they move together towards the cell nucleus.

dered diffusion in microdomains is illustrated further in the case of Thy-1 antigen diffusion (see below).

Complexes of 240-kD p-L-l Au40 Cell Surface Complexes Primarily Undergo Retrograde Movement Dependent on ATP and Microfilament Integrity

The 240-kD p-L-l Au40 behaved in an entirely different way when added to cultured cells (Fig. 2). These particles bound to the coverslip to the same extent as to the cell surface. Membrane-bound particles assumed fixed positions immediately after touching the cell surface. Time-lapse recordings of cells with free peripheral lamellae showed a centripetally oriented flow of the gold particles on the lamellae. At the transition zone between the thin peripheral parts (lamellopiasm) and the organelle-containing cytoplasm (endoplasm) this flow stopped and the gold particles accumulated in these

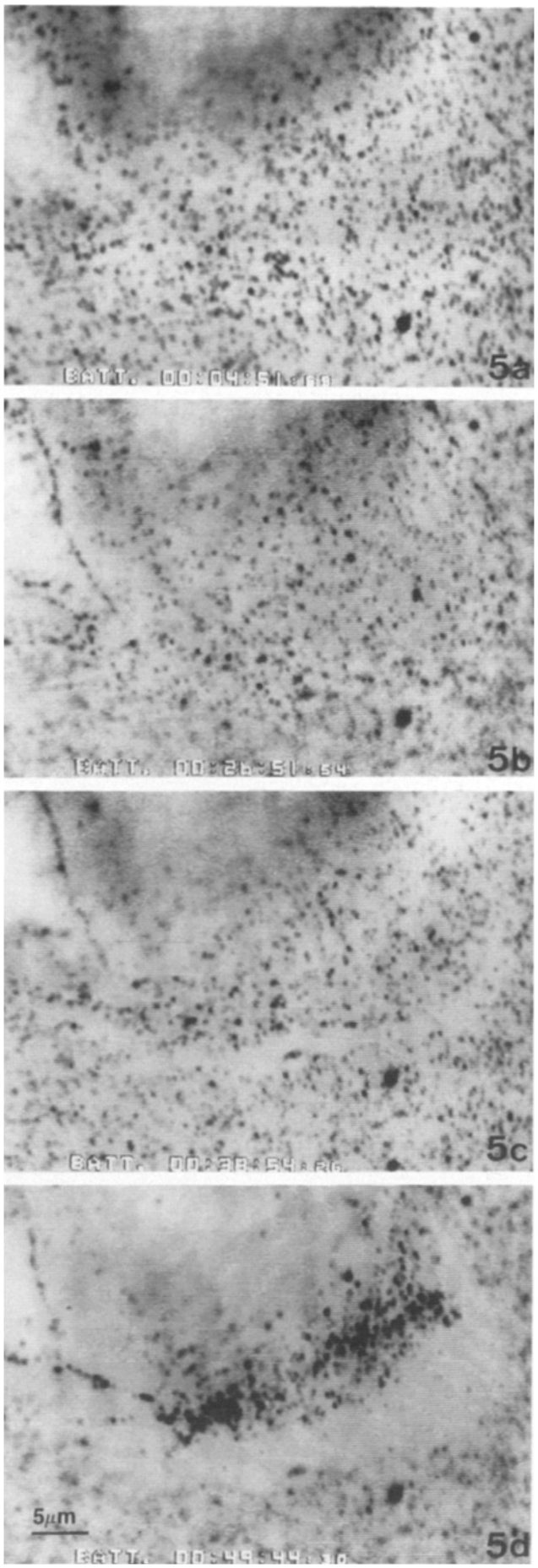

regions within 15–20 min. On the ventral cell surface (close to the coverslip) or on cells without free peripheral regions no flow or aggregation of particles was seen.

If the p-L-l concentration was altered, the behavior of the gold particles slightly changed. Gold particles treated with 1 mg/ml of the 240-kD p-L-l behaved the same way as the ones treated with 100 μg/ml. At 10 μg/ml of 240-kD p-L-l a small amount of the surface-bound particles showed two-dimensional Brownian motion.

To see which aspects of the dynamic behavior of p-L-l Au were dependent on the living state of the cells, monolayers were fixed before gold labeling, either with glutaraldehyde (1% for 10 min) or formaldehyde (4% for 20 min) and transferred to PBS containing 1 g/liter glucose at 37°C. Both fixatives gave identical results. 240-kD p-L-l Au40 particles all assumed fixed positions immediately after attaching to the cell surface. Label was evenly distributed on the entire cell surface, indicating a uniform distribution of binding sites before labeling. This remained so for long times. Internalized gold particles were detected by looking for saltatory motion rather than Brownian motion or retrograde movement on the live video image. It turned out that this internalization was much more frequent with this probe than with the 4-kD p-L-l Au. Although most gold particles remained on the surface for up to 2 h many more endocytic vesicles containing gold were seen (see Fig. 7 *b*). It was clear from the video images that internalization occurred preferentially at the transition zones between lamello- and endoplasm (possibly due to the high concentration of probes at that location).

When 240-kD p-L-l Au was added to cells that already had 4-kD p-L-l Au on their surface or vice versa, each population of membrane-bound particles behaved as in single-label experiments. The addition of the second gold probe had no effect on the dynamic behavior of the first. The behavior of the 240-kD p-L-l Au was reminiscent of the rearward movement of large particles on certain cell types (Abercrombie et al., 1970) and has been related to the movement of submembranous microfilament arcs (Heath, 1983). Therefore we investigated whether such an interaction could be relevant to our observation.

In the peripheral lamellae, it was obvious that there is a close relation between the cytoskeletal organization and the centripetral movement of the 240-kD p-L-l Au. In cells, fixed and stained for actin at different times after addition of the gold probe, the accumulation in the transition zone was in general closely related to the microfilament arc parallel to the leading edge and closest to the nucleus. No relationship existed with microtubules or with stress fibers that were arranged more or less orthogonally to the free cell border (Fig. 3).

When living cells were observed with video-enhanced

Figure 5. The effects of 1-h treatment with 10 mM sodium azide on the distribution of 240-kD p-L-l Au40. There is no evidence for aggregation as observed in other experimental conditions. The preparation is mounted on the microscope and continuously observed. During the first 20 min the distribution did not change (*a*). At 20 min the preparation was perfused with PBS supplemented with 1 mg/ml glucose to restore ATP levels. Gradually, retrograde flow resumes and aggregation becomes evident again (*b–d*).

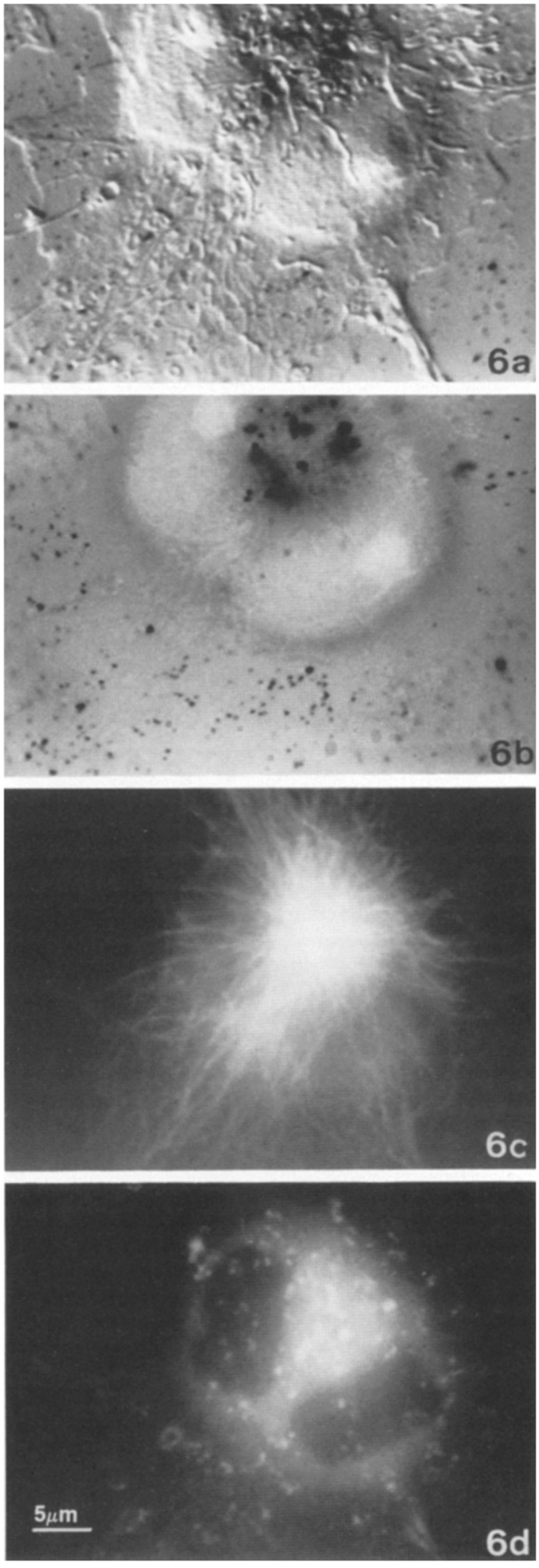

differential interference contrast microscopy, the movement of the microfilament arcs sometimes could be followed. These structures formed close to the leading edge and moved centripetrally until they reached the transition zones where they disappeared or were no longer discernible from other cellular structures. When 240-kD p-L-l gold was added to such cells the flow of surface-bound particles was closely associated with the centripetral flow of the arc-shaped microfilament bundles. Many particles remained apparently attached to an underlying arc throughout their centripetral movement (Fig. 4). Other particles located between two successive arcs migrated at the same velocity, suggesting that they were linked to a microfilament arc or sheet that could not be resolved. All particles finally accumulated in the region where the movement of the arcs became arrested.

To study the mechanism of the directed retrograde transport the influence of ATP depletion and cytoskeletal alterations was investigated. 240-kD p-L-l Au added to cells pretreated with 10 mM sodium azide did not migrate towards the transition zone by the typical centripetal flow. The majority of the surface-bound particles exhibited Brownian motion, although it was characterized by a lower diffusion coefficient than for the 4-kD p-L-l Au40 (Table III). Furthermore, no accumulations were formed either on the transition zones nor on intercellular contacts. At that point, the cells were perfused with PBS containing 1 g/liter glucose to restore the ATP levels. The Brownian motion ceased immediately and the centripetal flow resumed. Accumulations formed again on both transition zones and on intercellular contacts (Fig. 5).

On the other hand, when sodium azide was added to cells with 240-kD p-L-l Au which had accumulated on the cell surface for 20 min, particles started to move in a Brownian fashion resulting in a dispersion of the accumulations on cell–cell contacts and on transition zones. They gradually redistributed on the cell surface. In contrast, the mobility of the 4-kD p-L-l Au was not significantly altered by sodium azide pretreatment (Table III).

Disruption of the microtubule network by nocodazole (1 μg/ml, 24 h pretreatment) did not induce any changes in the binding or behavior of the p-L-l Au particles (data not shown). However, pretreatment of the cells with cytochalasin B (1 or 10 μg/ml for 24 h) markedly altered the behavior of the 240-kD p-L-l Au without affecting its binding to the cell surface. The majority of the membrane-bound particles now showed some limited Brownian motion. Time-lapse observation did not reveal any kind of flow. Large aggregates accumulated above the center of the cells, which often corresponded to

Figure 6. Video images of a PtK_2 cell, fixed 60 min after addition of 240-kD p-L-I Au40 pretreated with 1 μg/ml cytochalasin B for 24 h. (*a*) Nomarski interference contrast image. (*b*) Bright-field image, showing random distribution of colloidal gold probes. There is no evidence for the typical aggregation at the boundary between lamelloplasm and cytoplasm (see previous figures). (*c*) Immunofluorescence of antitubulin in this cell. The microtubule network is not modified. (*d*) Immunofluorescence of antiactinine, showing "patchy" appearance of microfilaments, induced by the cytochalasin treatment. Notice the large accumulations of colloidal gold above the nucleus, corresponding to dense actin aggregates.

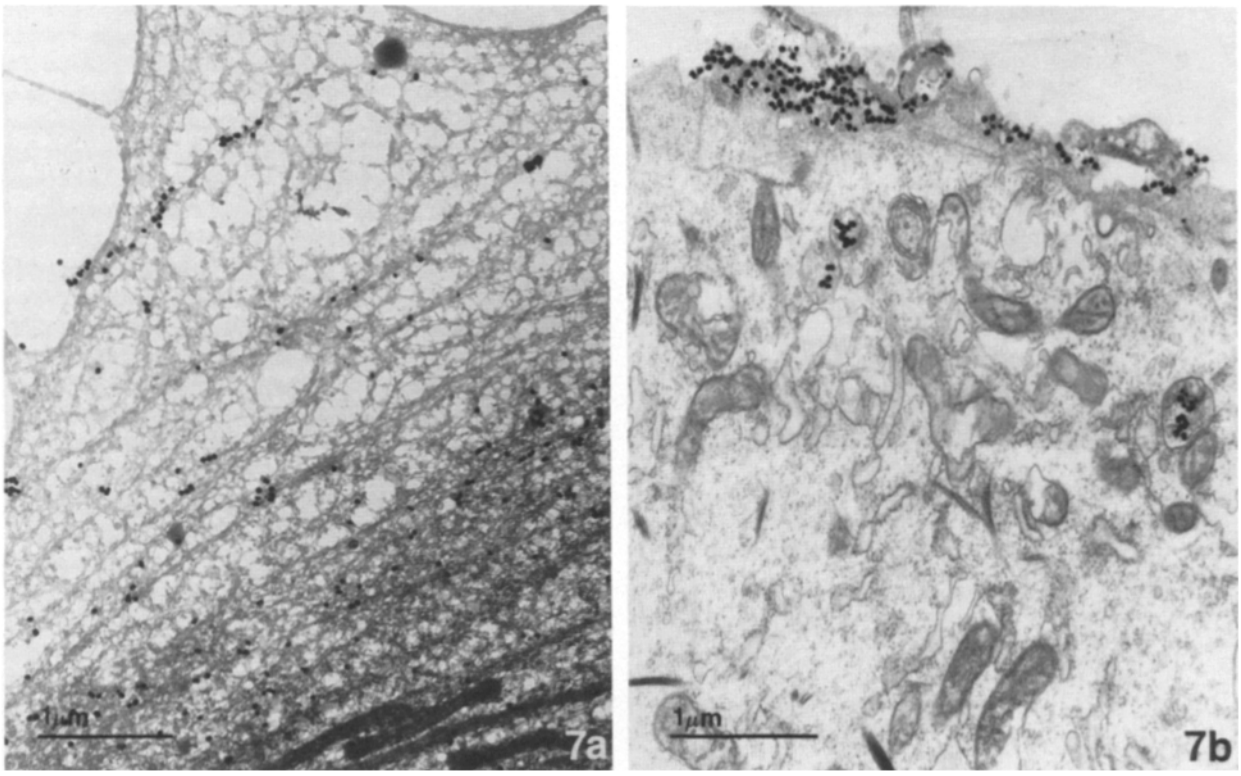

Figure 7. (*a*) Ultrastructural observation of 240-kD p-I-l Au40 after 10 min of incubation. The gold probes are clearly associated with microfilaments. (*b*) Another cell, fixed after 30 min of incubation. The aggregation is clearly visible. Some colloidal gold probes are contained in large endocytotic vesicles.

dense aggregates of antiactinin staining. Microfilament arcs could no longer be detected in these cells (compare Fig. 6 *d* and 4 *d*). Furthermore, the rate of internalization was appreciably faster than in untreated cells. The endocytosed particles accumulated in the juxtanuclear area. No accumulations were formed on intercellular contacts (Fig. 6). This shows that an intact microfilament organization is necessary for retrograde movement of the 240-kD p-L-l complexes.

The compounds that arrested the centripetal migration of the 240-kD p-L-l Au also affected the actin filament organization as visualized with immunofluorescence. Most notably, microfilament arcs could no longer be detected in cells treated with any of these compounds. In azide-treated cells, stress fibers became progressively fragmented leaving short fibers and actin-staining aggregates concentrated above the nucleus (data not shown). There was no relationship between gold particles and the remaining antiactin staining network, which replaced the stress fibers and arcs.

The involvement of microfilaments in the transport is further supported by ultrastructural evidence of cell surface gold particles in apparent association with underlying cytoskeletal elements (Fig. 7 *a*). Slight internalization was observed during the first hour after gold addition as observed with EM. Accumulation of gold particles were within internal membrane-bounded vesicles (Fig. 7 *b*). After 2 h, approximately half of the particles were internalized, while after 4 h the majority was located intracellularly and distributed in large endocytotic vesicles.

40-nm Au–anti-PGP-1 Antibody Complexes Are Capped Similar to 240-kD p-L-l Au40 Cell Surface Complexes

The behavior of the 240-kD p-L-l Au40 was compared to gold labeling of PGP-1, a major murine cell surface glycoprotein (Hughes et al., 1981).

40-nm colloidal gold, coupled either to a monoclonal antibody against PGP-1 or to 240-kD p-L-l Au40, bound avidly to the cell surface of MO cells, and displayed no motion when observed in real-time. However, in the time-lapse mode, a directed rearward motion of the probe became apparent (Fig. 8) with a velocity in the 0.5–1 μm/min range. The probe accumulated in specific areas, which because of the morphology of the cell were not clearly delineated as transition zones between cytoplasm and lamelloplasm. The uniform motion was also inhibited in a reversible way with 10 mM sodium azide (data not shown).

Au40–Thy-1 Antibody Complexes Diffuse Randomly But in Restricted Regions

The behavior of 4-kD p-L-l Au40 was compared with Thy-1, a lipid-linked glycoprotein (Tse et al., 1984; Gupta et al., 1988). A monoclonal antibody against the Thy-1 antigen (Ishihara et al., 1988) was coupled to 40-nm colloidal gold, and incubated with 3T3 fibroblasts. We investigated the effect of two different stabilization agents, BSA and a mixture of PVP and gelatin. With the BSA stabilization, binding was

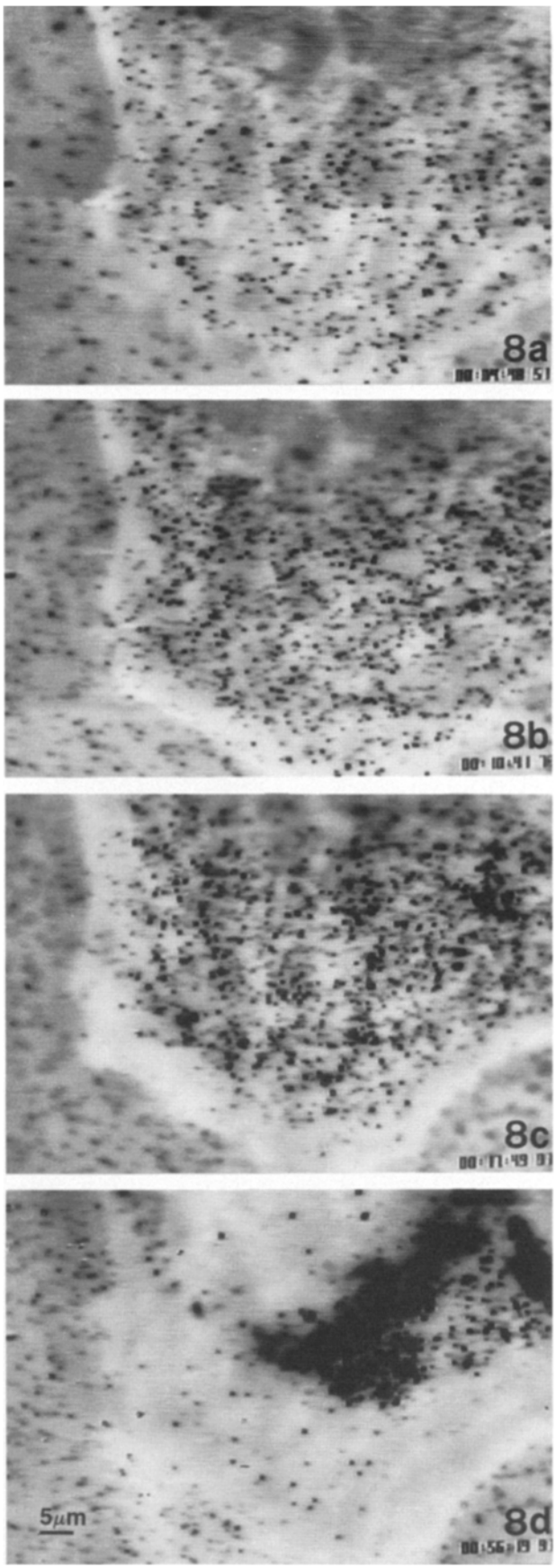

moderate, and ~50% of the gold probes remained immobile. These immobile probes generally had more contrast in the video image, suggesting that they were highly aggregated (Fig. 9 *a*). With the PVP–gelatin stabilization procedure, however, ~80% exhibited a Brownian motion with a calculated diffusion coefficient of 0.1–0.2 $\mu m^2/s$ (Fig. 9, *d* and *e*). The contrast of these gold probes was more uniform, suggesting much less aggregation of the gold particles.

The probes did not exhibit any uniform flow as judged by time-lapse observations. This observation is consistent with FRAP measurements on 3T3 cells (Ishihara et al., 1988). If one follows a single particle over time by the naked eye, one gets the impression that the movement of this particle is bounded in some way. Often a particle interrupts its jerky Brownian motion for several seconds, stays immobilized, and then resumes its motion. This behavior was observed on different cells. The suggestion of hindered diffusion is confirmed by a detailed analysis of the motion. Indeed, Fig. 9 shows in detail that this diffusion is somewhat spatially restricted, in apparent domains with a size between 0.7 and 2 μm.

We first calculate a diffusion coefficient of 0.1 $\mu m^2/s$ from the slope of the x^2 vs. T relation at time zero. Starting from this measured diffusion constant, we calculate that in 30 s about 32% of the particles should have moved in excess of $x = \sqrt{4Dt}$, or 3.5 μm from their starting points (Eq. 3). The real distance can be assessed by the areas covered by the particles and shown in the TRACE image. Fig. 9, *b* and *e*, shows the TRACE images observed over 30 s for two different label densities of the Thy-1 probe. Fig. 9 *c* displays the distribution of areas covered by the motion of some 75 individual particles during 30 s. Comparison with the expected distribution (Eq. 3) reveals the existence of apparent microdomains with 0.5–1 μm diameters.

In addition, the x^2 vs. T for individual particles should follow a linear relationship in the case of free diffusion. However, a real x^2 vs. T relation shows a downward reflection at values for x^2 between 1 and 3 μm (compare Fig. 9 *f* with Fig. 1 *f*). This suggests also restricted diffusion in microdomains of 1–2 μm.

Discussion

Binding and Mobility of 4-kD p-L-l Au Ligands in Relation to Thy-1 Gold Complexes

The reduced labeling of the 4-kD p-L-l Au probes, after treatment of the cells with neuraminidase of DMJ, suggests that the positively charged gold particles bind predominantly to negatively charged sialic acid residues of membrane glycoproteins and glycolipids. The substantial *Tx*-100–induced release of 4-kD p-L-l Au40 indicates that a large portion of the gold is bound to membrane components embedded in the lipid bilayer. The conclusion that 4-kD p-L-l Au40 predomi-

Figure 8. The PGP-1 glycoprotein behavior on the surface of 3T3 fibroblast is very similar to the directed motion of the 240-kD p-L-l Au40. (*a–d*) Different time points (observed in bright field) of the cell surface distribution. There is a clearing of the peripheral lamella and an accumulation in a zone near the cell nucleus.

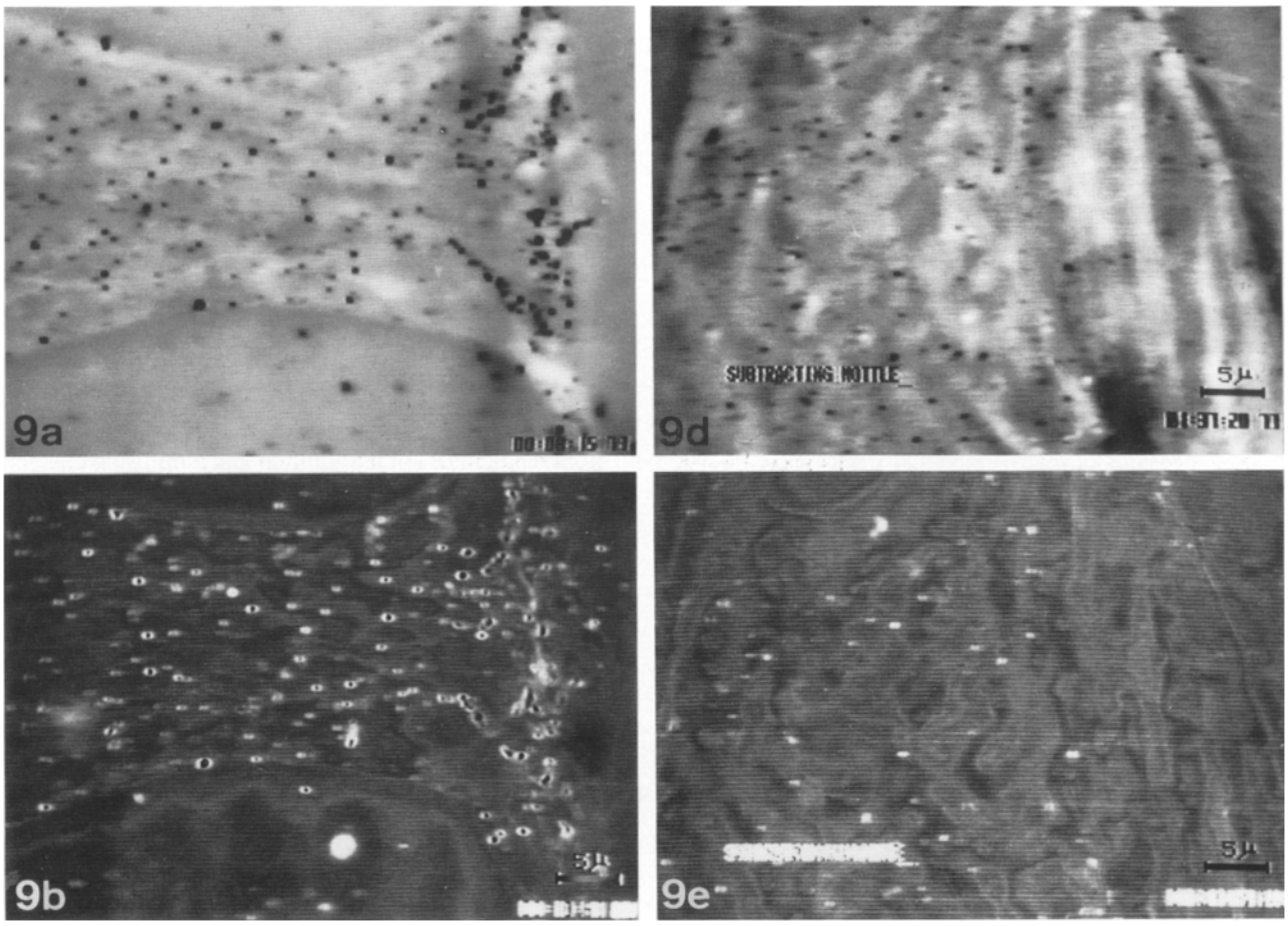

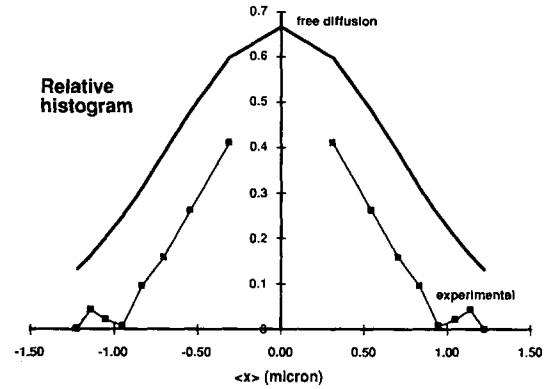

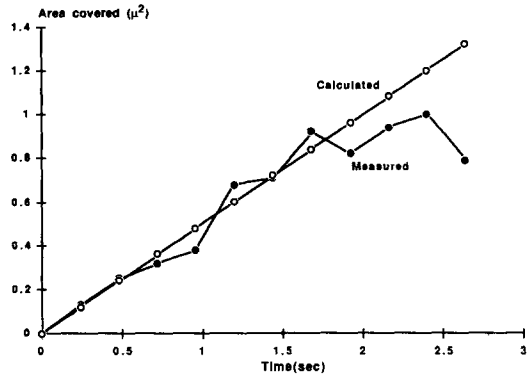

9c 9f

Figure 9. The behavior of two differently stabilized Thy-1 probes on 3T3 cells suggests restricted diffusion in conditions with different probe densities. (*a*) Bright-field image of a 3T3 cell, labeled with the BSA/PEG-stabilized Thy-1 gold probe. (*b*) TRACE image of this sequence over 30 s. The individual gold probes do not cover the whole surface. (*c*) Distribution of the areas covered over a time period of 30 s by all colloidal gold probes and calculated from the TRACE image. Comparison with the calculated distribution, assuming a calculated free diffusion coefficient of 0.1 $\mu m^2/s$, shows that diffusion is somewhat hindered or "corraled." (*d*) Bright-field image of the PVP-cold-water fish gelatin-stabilized Thy-1 probe on a 3T3 cell. (*e*) Trace image of this sequence over 30 s. Observe again the individual domains. (*f*) x^2 vs. relation of a single Thy-1 probe. Again, the effect of restricted diffusion is evident as a deflection in the curve at longer times.

nantly binds to membrane proteins is corroborated by its lateral mobility. Its diffusion coefficient is high, markedly temperature dependent, and does not depend on ATP. Indeed, 4-kD p-L-l Au has mobility characteristics similar to gold-labeled anti-Thy-1; this also suggests predominant binding to lipid components of the membranes since the lipid-linked Thy-1 glycoprotein exhibits high lateral mobility, characteristic of lipid analogues (Ishihara et al., 1987).

Diffusion coefficients of 4-kD and the Thy-1 probes are in the 0.1–0.3 $\mu m^2/s$ range, much larger than the diffusion coefficients of Con A–labeled gold (0.004–0.01 $\mu m^2/s$) (Sheetz et al., 1989). This probably reflects the fact that the majority of Con A receptors are membrane glycoproteins with lower diffusion coefficients. The Con A probe probably cross-links many glycoproteins, their motion resembling the motion of our 240-kD p-L-l probe. Uniform motion at this low velocity (0.5–1 $\mu m/min$) indeed can be assessed only accurately, when observed over many minutes. In addition, observation of the Con A–gold probes by Sheetz et al. (1989) was performed in the differential interference contrast mode, which is less sensitive to the visualization of individual gold probes. We provide clear evidence that the diffusion of the 4-kD p-L-l Au40 and the Thy-1 probes is spatially restricted. The x^2 vs. T behavior of many individual tracks show hindered diffusion at a scale of 1–2 μm. In addition, visualizing the motion of a large number of particles with the TRACE feature of the Hamamatsu image processor indicates that particles do not wander nearly as far as would be expected if their diffusion were free. This observation further agrees with the experiments of Sheetz et al. (1989) who found spatially restricted diffusion of Con A–labeled gold.

Restricted diffusion has been observed in earlier work on erythrocytes (He and Hui, 1985; Peters, 1988) and on mammalian sperm (Cowan et al., 1987). In addition, from the dependence of the immobile fraction on the beam radius of FRAP measurements of *N*-7-nitrobenz-2-oxa-1,3,diazol-4-yl amino-phosphatidylcholine, Yechiel and Edidin (1987) found evidence for protein-rich 1-μm domains in fibroblasts. In this regard, the observation that individual gold probes alternate diffusive motion with periods of immobilization suggest the association and dissociation of the probes with certain membrane or cytoskeleton elements, which somehow line the microdomain. This behavior is in line with the concept of temporary association and dissociation of mobile glycoproteins with an underlying cytoskeletal complex (Edelman, 1976).

These observations have extremely important implications for membrane structure; however, the challenge remaining lies in demonstrating that the apparent microdomains are not experimentally induced by the large gold particles themselves.

In principle, the observed immobile gold clusters in the Thy-1 experiment could arise from aggregate formation caused by the multivalency of the colloidal gold–antibody complex. Multivalent gold probes could interfere with the motion by cross-linking several epitopes. With the classical BSA stabilization methods, experiments in our lab have shown that ~25–30 antibodies are coupled to one 40-nm gold probe, the vast majority of which will not be able to bind the antigen. Recent developments in stabilization agents, which cover more efficiently the available gold surface, drastically reduce this number. It is therefore important in Nanovid microscopy to characterize the degree of multivalency of the gold probes.

In addition, steric hindrance of the gold labels themselves could, in principle, restrict movement. However, we provide evidence suggesting that the mobility of 4-kD p-L-l Au is in the same range as the values obtained from FRAP measurements on fluorescently labeled anti-Thy-1. Its diffusion coefficient is among the highest observed for membrane constituents. Only at the intercellular contact areas were immobile probes found. This shows that, at least for the short-range diffusion of the 4-kD p-L-l Au40 and the Thy-1 probe, interference from the large gold probe is negligible. If the observation of microdomains should be due to artificial cross-linking of colloidal gold labels, the notion of restriction Brownian motion should be dependent on gold density. The fact that we observed restricted Brownian motion at different densities suggests that the apparent microdomains are not induced by the gold probes themselves.

There is no evidence for directional flow (Bretscher, 1984) of the 4-kD p-L-l probe or the Thy-1 probe on the time scale of the experiment (1–2 h). In addition, when we calculate the ratio between the probe concentration at the leading edge (C_a) and a zone L 20 μm away (C_b) at equilibrium, for an observed flow (F) of 0.5 $\mu m/min$ and a diffusion coefficient (D) of 0.31 $\mu m^2/s$ (for the 4-kD p-L-l Au probe), we obtain a value of $C_a/C_b = \exp(-FL/D)$ or 0.63 (Bretscher, 1976). This means that in the model of lipid membrane flow, a fraction of $1/(1 + 0.63)$ or 62% of the particles should have moved towards the cell center. Over an observation period of 1–2 h, we found no evidence for this large segregation. The physiological implications of such diffusion in microdomains could be important. Indeed, binding of substrates to receptors and subsequent diffusion to an effector complex can be performed more efficiently when the mobility is restricted to small domains (Peters, 1988). In addition, compartmentalization of the cell membrane could enhance the rich variety of cellular responses to different stimuli by directing extracellular signals towards well-defined intracellular compartments. In neuronal cells, for instance, the extreme differentiation between dendrites and axons permits a tight coupling between electrical membrane events and intracellular effects (Angelides et al., 1988).

Binding and Mobility of 240-kD p-L-l Au Ligands in Relation to PGP-1–Au Complexes

The fact that 240-kD p-L-l Au complexes are largely determined insoluble suggests an association with the cytoskeleton; further support for this assertion comes from the ultrastructural evidence (Fig. 7 *a*). Certainly, the long p-L-l chains may serve to cross-link several membrane components and this cross-linking may induce coupling of the membrane complex to the cytoskeleton. The positively charged p-L-l molecules may bind to negatively charged glycoproteins and glycolipids as well as acidic phospholipids. Indeed, 240-kD p-L-l Au has been shown to interact strongly with model membranes, even inducing phase separation (Carrier et al., 1985; Laroche et al., 1988). Alternately, the cell surface may contain a small percentage of glycoproteins that are linked to the cortical cytoskeleton. The multivalent polylysine gold would then have a greater probability of binding to at least one such glycoprotein in addition to unlinked elements.

The rearward movement of 240-kD p-L-l Au probes on the leading lamellae of motile cells closely resembled the motion of the membrane glycoprotein PGP-1, patched by addition of cross-linking antibodies (Holifield et al., 1990; Holifield, B., and K. Jacobson, manuscript submitted for publication) suggesting that the 240-kD p-L-l Au probe is transported in a similar fashion.

The transmembrane linkage endows the markers with a

fixed position over much of the cell surface. On the peripheral edges, those membrane components are constantly swept backwards by a mechanism, probably involving linkage of aggregated membrane components to a rearward-moving, actin-based cortical cytoskeleton (Heath, 1983; Forscher and Smith, 1988) underlying the dorsal surface of the active lamella. This view is supported by our video microscopic and immunofluorescence data, the ultrastructural evidence, and the inhibition of transport by either ATP depletion or cytochalasin B. These data are consistent with other recent analyses of rearward particle transport (Fisher et al., 1988; Sheetz et al., 1989; Forscher and Smith, 1990); all of this data is compatible with a retrograde actin flow, as opposed to a rearward lipid flow (Bretscher, 1984), driving surface particle movements.

This account demonstrates that Nanovid microscopy is a powerful tool to follow the dynamic behavior of individual membrane components. The individual gold particles can be followed at high resolution and quantitative information can be obtained by computer analysis.

We thank Dr. N. DeJaeger (Agfa Gevaert) for lending his Pen-Kem Electrophoretic Laser Light Scattering setup. Valuable help was appreciated from Dr. J. Leunissen in the coupling of the antibodies to colloidal gold. The skillful photographic work of L. Leyssen and G. Jacobs is highly appreciated. We acknowledge the helpful comments of Dr. Greta Lee on the manuscript.

This work has been supported by a grant from Instituut voor Wetenschappelijke Ondersteuning van Landbouw en Nijverheid, Brussels, Belgium.

Received for publication 17 July 1990 and in revised form 29 August 1990.

References

Abercrombie, M., J. Heaysman, and S. Pergrum. 1970. The locomotion of fibroblasts in culture. III. Movements of particles on dorsal surface of the leading lamella. *Exp. Cell Res.* 60:437–444.

Angelides, K., L. Elmer, D. Loftus, and E. Elson. 1988. Distribution and lateral mobility of voltage-dependent sodium channels in neurons. *J. Cell Biol.* 106:911–925.

Bretscher, M. 1976. Directed lipid flow in cell membranes. *Nature (Lond.).* 260:21–22.

Bretscher, M. 1983. Distribution of receptors for transferrin and low density lipoprotein on the surface of giant HeLa cells. *Proc. Natl. Acad. Sci. USA.* 80:454–458.

Bretscher, M. 1984. Endocytosis: relation to capping and cell locomotion. *Science (Wash. DC).* 224:681–686.

Carrier, D., J. Dufourcq, J. F. Faucon, and M. Pezolet. 1985. A fluorescence investigation of the effect of polylysine on dipalmitoylglycerol bilayers. *Biochim. Biophys. Acta.* 820:131–139.

Cowan, A., D. Myles, and D. Koppel. 1987. Lateral diffusion of the PH-20 protein on guinea pig sperm: evidence that barriers to diffusion maintain plasma membrane domains in mammalian sperm. *J. Cell Biol.* 104:917–923.

Crank, J. 1974. The Mathematics of Diffusion. Clarendon Press, Oxford, UK. p. 29.

de Brabander, M., G. Geuens, R. Nuydens, M. Moeremans, and J. de Mey. 1985. Probing microtubule dependent intracellular motility with nanometer particle video ultramicroscopy. *Cytobios.* 43:273.

de Brabander, M., R. Nuydens, G. Geuens, M. Moeremans, and J. de Mey. 1986. The use of submicroscopic gold particles combined with video contrast enhancement as a simple molecular probe for the living cells. *Cell Motil. Cytoskeleton.* 6:105.

de Brabander, M., R. Nuydens, H. Geerts, and C. Hopkins. 1988. Dynamic behavior of the transferrin receptor followed in living epidermoid carcinoma cells (A431) with Nanovid microscopy. *Cell Motil. Cytoskeleton.* 9:30–47.

de Brabander, M., H. Geerts, R. Nuydens, and R. Nuyens. 1989. Detection of gold probes with video-enhanced contrast microscopy: Nanovid microscopy. *Am. J. Anat.* 185:282–295.

de Brabander, M., R. Nuydens, H. Geerts, and R. Nuyens. 1989. Detection and use of gold probes with video-enhanced contrast light microscopy. *In* Immunogold Staining in Cell Biology. A. Verkleij, and J. Leunissen, editors. *CRC* 217–232.

Dembo, M., and A. Harris. 1981. Motion of particles adhering to the leading lamella of crawling cells. *J. Cell Biol.* 91:528–536.

De Mey, J. 1984. Colloidal gold probes in immunochemistry. Practical applications in pathology and biology. J. Polak and S. van Noorden, editors. *Wright PSG, London.* 82–112.

Edelman, G. 1976. Surface modulation in cell recognition and growth. *Science (Wash. DC).* 192:218–226.

Fisher, G., P. Conrad, R. DeBiaiso and D. Taylor. 1988. Centripetal transport of cytoplasm, actin and the cell surface in lamellipodia of fibroblasts. *Cell Motil. Cytoskeleton.* 11:235–247.

Forscher, P., and S. Smith. 1988. Actions of cytochalasins on the organization of actin filaments and microtubules in a neuronal growth cone. *J. Cell Biol.* 107:1505–1516.

Forscher, P., and S. Smith. 1990. Cytoplasmic actin filaments move particles on the surface of a neuronal growth cone. *In* Optical Microscopy in Biology. B. Herman and K. Jacobson, editors. Alan R. Liss, Inc., New York. In press.

Fuhrmann, U., B. Bause, and H. Ploegh. 1985. Inhibitors of oligosaccharide processing. *Biochim. Biophys. Acta.* 825:95–110.

Geerts, H., M. de Brabander, R. Nuydens and R. Nuyens. 1987*a*. Nanovid correlation spectroscopy: quantitative analysis of cell surface motility with poly-lysine coated gold probes. *Proc. IX Int. Biophys. Congr., Jerusalem.* p. 125.

Geerts, H., M. de Brabander, R. Nuydens, S. Geuens, M. Moeremans, J. De Mey and P. Hollenbeck. 1987*b*. Nanovid tracking: a new automatic method for the study of mobility in living cells based on colloidal gold and video microscopy. *Biophys. J.* 52:775–782.

Goldstein, B., and F. Wiegel. 1988. The distribution of cell surface proteins on spreading cells: comparison of theory with experiment. *Biophys. J.* 53:175–184.

Grahame, D. 1947. The electrical double layer and the theory of electrocapillary. *Chem. Rev.* 44:441–501.

Gross, D., and W. Webb. 1986. Molecular counting of low-density lipoprotein particles as individuals and small clusters on cell surfaces. *Biophys. J.* 49:901–911.

Gupta, D., A. Tartkoff, and E. Tisdale. 1988. Metabolic correction of defects in the lipid anchoring of Thy-1 in lymphoma mutants. *Science (Wash. DC).* 242:1446–1448.

Harris, A., and G. Dunn. 1972. Centripetal transport of attached particles on both surfaces of moving fibroblasts. *Exp. Cell Res.* 73:519–523.

He, N., and S. Hui. 1985. Electron microscopic observation of domain movement in reconstituted erythrocyte membranes. *Proc. Natl. Acad. Sci. USA.* 82:7304–7308.

Heath, J. 1983. Behavior and structure of the leading lamella in moving fibroblasts: occurrence and centripetal movement of arc-shaped microfilament bundles beneath the dorsal cell membrane. *J. Cell Sci.* 60:331–354.

Holifield, B., A. Ishihara, J. Lee, and K. Jacobson. 1990. Movement of plasma membrane components during cell locomotion. *In* Optical Microscopy in Biology. B. Herman and K. Jacobson, editors. Alan R. Liss Inc., New York. In press.

Hughes, E., G. Mengod, and T. August. 1981. Murine cell surface glycoproteins: characterisation of a major component of 80,000 daltons as a polymorphic differentiation antigen of mesenchymal cells. *J. Biol. Chem.* 256:7023–7027.

Ishihara, A., Y. Hou, and K. Jacobson. 1987. The Thy-1 antigen exhibits rapid lateral diffusion in the plasma membrane of rodent lymphoid cells and fibroblasts. *Proc. Natl. Acad. Sci. USA.* 84:1290–1293.

Isihihara, A., B. Holifield, and K. Jacobson. 1988. Analysis of lateral redistribution of a monoclonal antibody complex plasma membrane glycoprotein which occurs during cell locomotion. *J. Cell Biol.* 106:329–343.

Kilmartin, J., B. Wright, and C. Milstein. 1982. Rat monoclonal antitubulin antibodies derived by using a new nonsecreting rat cell line. *J. Cell Biol.* 93:576–582.

Kucik, D., E. Elson and M. Sheetz. 1989. Forward transport of glycoproteins on leading lamellipodia in locomoting cells. *Nature (Lond.).* 340:315–317.

Langanger, G., J. de Mey, M. Moeremans, J. Small, and M. de Brabander. 1984. Immunoelectron microscopical localization of actin, α-actin and filamin with the IGS-method in chicken embryo lung epithelial cells. *J. Submicrosc. Cytol. Pathol.* 16:43–45.

Laroche, G., D. Carrier, and M. Pezolet. 1988. Study of the effect of poly(l-lysine) on phosphatidic acid and phosphatidylcholine/phospahtidic acid bilayers by Raman spectroscopy. *Biochemistry.* 27:6220–6228.

Peters, R., J. Peters, K. Tews, and W. Bahr. 1974. A microfluorometric study of translational diffusion in erythrocyte membranes. *Biochem. Biophys. Acta.* 367:282–294.

Peters, R. 1988. Lateral mobility of proteins and lipids in the red cell membrane and the activation of adenylate cyclate by β-adrenergic receptors. *FEBS (Fed. Eur. Biochem. Soc.) Lett.* 234:1–7.

Peters, R., and R. Cherry. 1982. Lateral and rotational diffusion of bacteriorhodopsin in lipid bilayers: experimental test of the saffman-Delbruck equations. *Proc. Natl. Acad. Sci. USA.* 79:4317–4321.

Sheetz, M., S. Turney, H. Qian, and E. Elson. 1989. Nanometre-level analysis demonstrate that lipid flow does not drive membrane glycoprotein movements. *Nature (Lond.).* 340:284–288.

Skutelsky, E., and J. Roth. 1986. Cationic colloidal gold – a new probe for the detection of anionic cell surface sites by electron microscopy. *J. Histochem.*

Cytochem. 34:693–696.
Sternberg, S. 1986. Grayscale morphology. *Computer vision, graphics and image processing.* 35:335.
Tse, A., D. Barclay, N. Watts, and A. Williams. 1984. A glycophospholipid tail at the carboxyl terminus of the Thy-1 glycoprotein of neurons and thymocytes. *Science (Wash. DC).* 230:1003–1005.
Verkleij, A., and J. Post. 1987. Physicochemical properties and organization of lipids in membranes: their possible role in myocardial injury. *Basic Res. Cardiol.* 82 (Suppl. 1):85–92.
Yechiel, E., and M. Edidin. 1987. Micrometer-scale domains in fibroblast plasma membranes. *J. Cell Biol.* 105:755–760.